Jamming Distance Dictates Colloidal Shear Thickening

Shravan Pradeep,[1] Mohammad Nabizadeh,[2] Alan R. Jacob,[1] Safa Jamali,[2] and Lilian C. Hsiao[1,*]
[1]Department of Chemical and Biomolecular Engineering, North Carolina State University, Raleigh, North Carolina 27695, USA
[2]Department of Mechanical and Industrial Engineering, Northeastern University, Boston, Massachusetts 02115, USA

(Received 3 July 2020; revised 10 May 2021; accepted 30 August 2021; published 6 October 2021)

We report experimental and computational observations of dynamic contact networks for colloidal suspensions undergoing shear thickening. The dense suspensions are comprised of sterically stabilized poly (methyl methacrylate) colloids that are spherically symmetric and have varied surface roughness. Confocal rheometry and dissipative particle dynamics simulations show that the shear thickening strength β scales exponentially with the scaled deficit contact number and the scaled jamming distance. Rough colloids, which experience additional rotational constraints, require an average of 1.5–2 fewer particle contacts as compared to smooth colloids, in order to generate the same β. This is because the surface roughness enhances geometric friction in such a way that the rough colloids do not experience a large change in the free volume near the jamming point. The available free volume for colloids of different roughness is related to the deficiency from the maximum number of nearest neighbors at jamming under shear. Our results further suggest that the force per contact is different for particles with different morphologies.

DOI: 10.1103/PhysRevLett.127.158002

Dense suspensions of colloidal particles with stochastic Brownian motion exhibit shear thickening under flow, a non-Newtonian behavior where the suspension viscosity η increases mildly or strongly depending on the applied shear stress σ and particle volume fraction ϕ. The ability to design the onset of shear thickening σ^* provides a unique advantage in the reversible tuning of material mechanics, which is of great interest in fields such as soft robotics, impact resistant fabrics, and liquid manufacturing [1–3]. However, the tunability in these systems currently remains at a rudimentary level of "on" or "off." For dense suspensions to truly advance technology, the level of control over the shear thickening needs to become more deliberate and refined [4,5]. In this Letter, we show that designing shear thickening strength is possible for a broad class of colloidal suspensions through a singular parameter: the distance to jamming.

A jammed material at ϕ_J is conventionally defined as a disordered particulate system that has developed a yield stress [6]. Shear thickening shares similarities to jamming in that the particles in a flowing suspension become impeded by the nearest neighbors and therefore require an increasing amount of stress to continue flowing [1,7]. The microstructural origin of shear thickening was first attributed to the formation of hydroclusters in Stokesian dynamics simulations [8]. Experiments later corroborated this observation [9], suggesting that the shear thickening onset can be discussed in the context of the dimensionless Péclet number ($\mathrm{Pe}_{sh} = 6\pi\eta a_{\mathrm{eff}}^3\dot{\gamma}/k_BT$), that represents the ratio of hydrodynamic to thermal forces acting on colloids, or through a dimensionless shear stress that accounts for the average force it takes to push particles into load-bearing contact [38]. More recently, simulations that incorporate explicit interparticle friction μ or particle roughness plus lubrication hydrodynamics were able to fully capture the large increase in viscosity that is characteristic of strong shear thickening [10,11]. An important result from these simulations is the appearance of space-spanning force chains and velocity correlations in shear thickened suspensions [12]. These force chains arise from combinations of σ- and ϕ-based constraints including hydrodynamics, repulsion, adhesion, and solid contact friction [11,13,14]. As Pe_{sh} increases, the force chains proliferate and grow stronger as a system undergoes stronger shear thickening and ultimately shear jamming [15]. Interestingly, conventional microstructural characterization techniques such as the radial distribution function [14] or scattering patterns in the velocity-gradient-vorticity planes [16] are not too sensitive to differences between shear thickened states. As $\phi \to \phi_J$ and σ increases, conservation laws state that the contact distance between particles in a constant-volume suspension must decrease, leading to a greater number of nearest contacts. To address a lack of experimental evidence of contacts chains in the literature, we focus on the microstructural characterization of dynamic contact networks formed by dense colloidal suspensions in shear thickening flows. Here, contact does not necessarily mean solid friction, but could be from interparticle and hydrodynamic forces that constrain particles into a stress-bearing network.

We use the mean contact number $<z>$, a measure for the number of contacting nearest neighbors around particles, to quantify the suspension microstructure because of the strong correlation of $<z>$ with bulk mechanics [17]. The contact

number at jamming, z_J, and ϕ_J are inextricably linked to the interparticle friction in dense packings. Application of Maxwell's isostatic criterion to a frictionless hard sphere system at $\phi_J = 0.64$ reveals that $z_J = 6$. Incorporating μ between colloids further reduces ϕ_J and z_J [18,19]. The rotational constraint μ is featured in several constitutive equations, particle simulations, and phenomenological models that describe shear thickening as due to particles undergoing a stress-induced lubricated-to-frictional transition beyond σ^* [20–22]. Additionally, experimental measurements demonstrate that the rotational dynamics of shape-symmetric particles with protrusions deviate significantly from simulations of hard sphere suspensions [23–26]. While the interparticle friction may not always track with surface roughness because of complex tribological factors (e.g., elastohydrodynamics [27,28]), in general, rougher particles have larger values of μ.

To investigate the role of surface roughness on the contact microstructure of shear thickening colloidal suspensions, we use confocal rheometry experiments and dissipative particle dynamics (DPD) simulations to identify a quantitative link between the strength of thickening $\beta = \log(\Delta\eta)/\log(\Delta\sigma)$ and the distance from jamming $(\phi_{\max} - \phi)/\phi_{\max} = \Delta\phi/\phi_{\max}$ for smooth and rough colloids. Physically, the parameter β represents the ensemble average change in viscosity and microstructure associated with an increasing stress. Here, $\phi_{\max}$ refers to the maximum jamming fraction for a disordered packing, where $\phi_{\max} = \phi_J(\sigma = 0\ \text{Pa})$ is obtained from confocal microscopy performed on colloids that have undergone unperturbed sedimentation under gravitational stress for three months. We obtain β using the average slope at the inflection points above σ^* and before the high shear plateau. At $\phi_{\max}$, the suspension is considered mechanically rigid and the suspension is not flowable at or beyond this ϕ. The value of $\phi_{\max}$ is verified independently within an experimental uncertainty of $\pm 5\%$ by fitting the relative low-shear viscosity ($\eta_{r,\text{low-shear}}$) divergence to the form $\eta_{r,\text{low shear}} = (1 - \phi/\phi_{\max})^{-2}$. The value of $\phi_{\max}$ is a key parameter in normalizing the jamming distance and varies for colloids with different surface morphologies.

We hypothesize that there is a universal correlation between $\Delta\phi/\phi_{\max}$, β, and $<z>$ for all suspensions exhibiting shear thickening. To reveal this relationship, we synthesize spherically symmetric and size-monodisperse poly(methacrylate) (PMMA) microspheres with different levels of surface roughness [29]. These particles are sterically stabilized with poly(12-hydroxystearic acid) (PHSA) brushes of lengths 10–15 nm [30]. We prepare suspensions at $\phi < \phi_{\max}$ by first centrifuging the stock suspension at a gravitational Péclet number, $\text{Pe}_g = 1500$ ($\text{Pe}_g = 4\pi a_{\text{eff}}^4 \Delta\rho g/3k_BT$), and subsequently diluting the shear jammed sediments with known volumes of an index-matched solvent, squalene. We obtain ϕ by imaging the fluorescent colloids with confocal laser scanning microscopy (CLSM, Leica SP8) and processing the 3D image volumes using a brightness-weighted centroid-based algorithm [31]. Separately, steady shear rheological measurements are performed using a stress-controlled rheometer (TA Instruments DHR-2) fitted with a 50-mm sandblasted cone-and-plate geometry.

Figure 1 shows different rheological behavior of PMMA hard colloids with two types of morphology and similar effective swollen diameters $2a_{\text{eff}}$, smooth [S, $2a = 1.65\ \mu\text{m} \pm 4\%$, Fig. 1(a)] and rocky [RK, $2a_{\text{eff}} = 1.49\ \mu\text{m} \pm 6\%$, Fig. 1(b)]. Two other morphologies are also studied: slightly rough (SR, $2a_{\text{eff}} = 1.86\ \mu\text{m} \pm 5\%$) and very rough (VR, $2a_{\text{eff}} = 1.47\ \mu\text{m} \pm 6\%$) [32]. These steady shear flow curves describe the relative suspension viscosity ($\eta_r = \eta/\eta_s$, squalene viscosity $\eta_s = 0.012\ \text{Pa} \cdot \text{s}$) as a function of scaled σ. The dotted lines represent the two stress points at which we obtain $<z>$ values from dynamic packings: one at $\tilde{\sigma} = \tilde{\sigma}_{\beta=0} < \tilde{\sigma}^*$ and the second at $\tilde{\sigma} = \tilde{\sigma}_\beta > \tilde{\sigma}^*$, where the overhead $\sim$ represents the stress values scaled by a_{eff}^3/k_BT. As $\tilde{\sigma} > \tilde{\sigma}^*$, there is an proliferation of interparticle contacts [21,33].

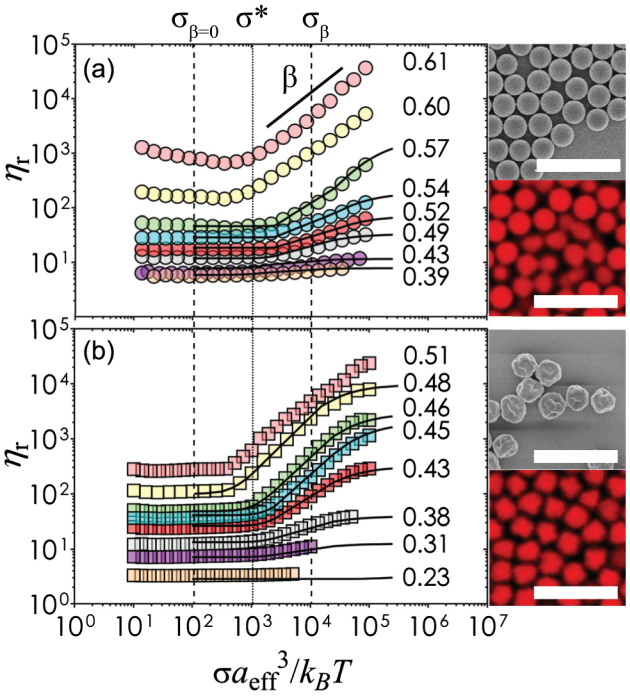

FIG. 1. Experimental rheology for suspensions of (a) smooth and (b) rough colloids. Flow curves represent η_r plotted against σ scaled by the effective particle radii and temperature. Numerical values next to each curve indicate the ϕ (filled). Solid lines are fits with the WC theory [20,34,35]. The vertical dashed lines represent the stresses below and above the onset stress (vertical dotted line) where we obtain the average contact numbers. Representative scanning electron micrographs and confocal micrographs of the colloids are shown to the right side of respective flow curves. Scale: 5 μm.

The suspensions transition from fully Newtonian flow at low σ and ϕ, to continuous shear thickening (CST, $\beta < 1$) at intermediate ϕ, and finally to discontinuous shear thickening (DST, $\beta \geq 1$) at high σ and as $\phi \to \phi_{\max}$. Some suspensions also exhibit a secondary plateau at the highest values of σ [11,14,19,21,36]. The onset of DST for smooth particle suspensions occurs at $\phi = 0.57$ [Fig. 1(a)], similar to the values reported earlier in the literature for colloids interacting with a short-range repulsive potential [34,37].

Our data show that $\Delta\phi/\phi_{\max}$ predicts β for different types of colloidal suspensions containing spherically symmetric particles. Figure 2 shows that all colloidal suspensions obey the general scaling of the form, $\beta \sim \exp(-\Delta\phi/\phi_{\max})$, where DST is present at $\Delta\phi/\phi_{\max} \leq 0.1$ and CST is found at $\Delta\phi/\phi_{\max} > 0.1$. The value of β rapidly decreases at increasing $\Delta\phi/\phi_{\max}$. Additional support for this correlation comes from β and $\Delta\phi/\phi_{\max}$ values extracted from a number of experiments and simulations in the literature [11,19,22,33,34,36,38–41]. This scaling has significant impact in the academic and industrial communities because it enables the *a priori* estimation of β (a dynamic stress-structure parameter) using $\Delta\phi/\phi_{\max}$ (a static configuration parameter). The remarkable match from independent research groups suggests that there exists a direct link between the shear thickening microstructure of colloids and their respective jamming distance. This link is more clearly illustrated using the dynamic $<z>$ values of shear thickening suspensions and their relation to $\Delta\phi/\phi_{\max}$.

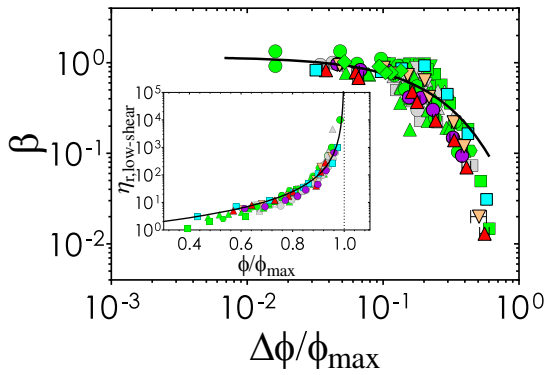

FIG. 2. Shear thickening strength as a function of jamming distance. Data from this work are shown in *S* (magenta circles), SR (red upper triangles), VR (coral lower triangles), and RK (cyan squares) colloids. Solid line indicates an empirical fit of the form: $\beta = \beta_0 \exp(-\Delta\phi/\phi_{\max}\kappa)$ with $\beta_0 = 1.61 \pm 0.05$ and $\kappa = 4.18 \pm 0.32$. Literature values from experimental colloidal studies are indicated by green symbols: smooth PMMA (circle) [34], rough PMMA (upper triangle) [38], smooth silica (square [41] and hexagon [36]), and rough silica (lower triangle [39] and diamond [40]). Literature values from simulations are indicated by gray symbols: colloids with surface asperities interacting via lubrication (square) [11], spheres with sliding friction (upper triangle) [22], spheres with sliding and rolling friction (circle) [19], and colloids interacting via sliding friction (lower triangle) [33]. Inset shows the fitting to the form: $\eta_r = (1 - \phi/\phi_{\max})^{-2}$ normalized for each particle $\phi_{\max}$ values. Solid line represents the universal low-shear viscosity divergence.

To characterize the contact microstructure of dense suspensions at the large applied stresses used to induce shear thickening, we use a custom confocal rheometer setup [Fig. 3(a)], where a stress-controlled rheometer (Anton Paar MCR 502 WESP) is directly coupled to a confocal laser scanning microscope (CLSM) (Leica SP8) similar to an earlier setup in the literature [42]. Steady shear is applied to suspensions of smooth and rough colloids using a 20 mm parallel-plate top geometry and a glass coverslip at the bottom (thickness = 0.17 mm). The confocal rheometer is used to obtain 3D image volumes of dense suspensions undergoing steady shear at $\tilde{\sigma}_{\beta=0}(\approx 10^2)$ and $\tilde{\sigma}_{\beta}(\approx 10^4)$, as described in Fig. 1. Each stack of size $50\ \mu\text{m} \times 50\ \mu\text{m} \times 10\ \mu\text{m}$ is imaged in under 5 s and contain $\sim 10^3 - 10^4$ particles. The suspensions contain

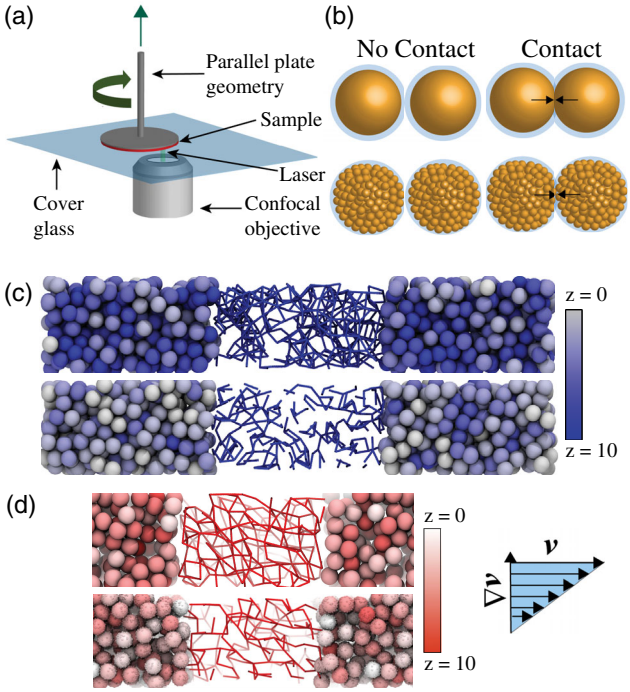

FIG. 3. (a) Confocal rheometer setup for imaging shear-induced contact networks during the flow measurements. (b) Schematic for interparticle contact in smooth (top row) and rough (bottom row) colloids. The light blue circle represents associated experimental length scales. (c),(d) Contact networks of shear thickening suspensions at $\Delta\phi/\phi_{\max} = 0.075$ and $\beta = 0.85$ as shown in VMD reconstructions of the (c) experimental microstructures and (d) simulation snapshots. For (c) and (d), the top panels are for the smooth particle suspensions and the bottom panels are for rough colloidal suspensions. Side insets show color panel for the respective z of the particles shown in (c),(d). Additional right inset represents the velocity-velocity gradient flow direction with respect to the contact networks shown in (c),(d).

5 wt% photocrosslinking mixture to rapidly arrest the suspensions with ultraviolet (UV) light within 1 s [43]. To obtain the sheared microstructure, we hold the suspensions at constant stresses, at values as marked in Fig. 1, for 150 s. We shine UV light ($\lambda_{exc} = 405$ nm) first and immediately drop the stress to zero ($\Delta t = 1$ s), thus locking in the suspension microstructure without any relaxation of the sheared structures (video_S1 in the Supplemental Material [43]). We perform three independent experiments and obtain image stacks from three different points in each sheared sample. All image stacks are imaged at least 15 μm above the coverslip to avoid wall effects.

The images obtained from the confocal rheometer experiments are supported using DPD simulations of bidisperse suspensions (a and $1.1a$ in an equal volume ratio with total number of particles $N = 1000$) containing smooth and rough colloids closely representing the experimental system [43]. The particle roughness is modeled by distributing asperities of length scale $0.1a$ on the surface of the smooth base spheres, similar to earlier simulations schemes [11,14,38,44–48]. To enable a proper comparison between simulations and experiments, the ϕ_{max} values for the simulated suspensions are matched to the S and RK experimental systems. The goal is to link β to $<z>$ and to capture the contact networks responsible for shear thickening.

Defining interparticle contact during shear thickening requires the use of two different contact criteria at $\tilde{\sigma} < \tilde{\sigma}^*$ and at $\tilde{\sigma} \geq \tilde{\sigma}^*$, because the particles undergo a transition from lubricated-to-frictional flow and the soft PHSA brush becomes compressed by the large applied stresses [38]. At $\tilde{\sigma} < \tilde{\sigma}^*$, two particles are defined to be in hydrodynamic contact if the interparticle separation is equal or less than the uncertainties that include the PHSA brush length, size polydispersity, and surface roughness [29]. At $\tilde{\sigma} \geq \tilde{\sigma}^*$, a frictional contact is defined by the average center-to-center distance between particles, $2a_{eff}$ as shown in Fig. 3(b) [44]. Thin layers of fluid could still be present between these frictional contacts. In DPD simulations, interparticle contacts are defined similarly for all particles and their interactions with other asperities and base particles. Experimental results are in excellent agreement with the contact microstructure obtained from DPD simulations for smooth and rough particles: the $<z>$ values obtained from DPD simulations fall within the error limits of the $<z>$ values obtained from our experimental packings, as shown in Fig. 4(a).

Visual molecular dynamics (VMD) renderings of the dynamic packings, at $\tilde{\sigma}_\beta$, from the experiments and simulations for suspensions containing smooth and rough particles at $\Delta\phi/\phi_{max} = 0.075$ and $\beta = 0.85$ are shown in Figs. 3(c)–3(d). The renderings show the presence of space-spanning contact networks and provide a statistical view of how smooth and rough colloids pack differently in shear thickening flows. Particles are concentrated in the compressive flow axis, in agreement with previous neutron scattering studies on shear thickening suspensions [16,49]. A first step towards constructing a mean-field description parameter of the contact microstructure formed in such networks would be possible by evaluating the relationship between the dynamic contact number at $\tilde{\sigma}_\beta$ and β for suspensions at various ϕ.

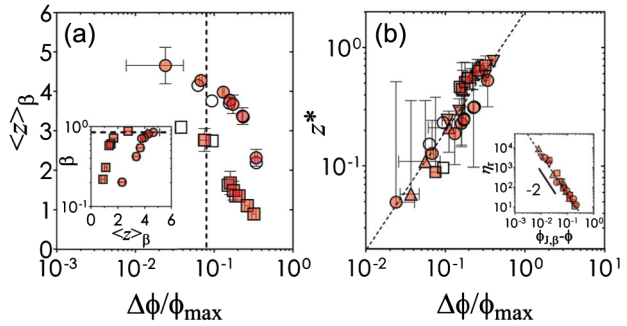

FIG. 4. (a) The change in $<z>_\beta$ of smooth (circles) and rough (squares) colloids from experiments (filled) and simulations (unfilled) as a function of $\Delta\phi/\phi_{max}$. Inset shows β as a function of $<z>_\beta$. Dashed lines in the main figure and the inset corresponds to the suspensions at $\Delta\phi/\phi_{max} = 0.075$ and $\beta = 0.85$. (b) The scaling $z^* \sim (\Delta\phi/\phi_{max})^\alpha$ obtained from experiments and simulations. Dashed line indicates the power law fit. Inset shows the scaling relation between η_r and unscaled jamming distance in accordance to $\eta_r \sim (\phi_{J,\beta} - \phi)^{-2}$. Two additional types of rough particles: SR (upper triangles) and VR (lower triangles) are included in (b).

Figure 4(a) shows the dynamic contact number, $<z>_\beta$, as a function of $\Delta\phi/\phi_{max}$ for sheared suspensions of smooth and rough colloids. The dashed lines in Fig. 4(a) indicate that the smooth colloids, on average, require 1.5–2 additional contacts to maintain the same β as compared to the rough colloids. The value of $<z>_\beta$ is a function of $\tilde{\sigma}_\beta$ because the external deformation imparts an additional nonequilibrium free energy that must be minimized for steady flow [50]. To normalize the spatial effect of interparticle contacts that stem from free volume differences, we define a parameter z^* that captures the scaled contact deficit, where $z^* = (z_{J,\beta} - <z>_\beta)/z_{J,\beta}$. Here, $z_{J,\beta}$ is the maximum possible contacts at $\phi_{J,\beta}$, which is defined as the divergence of the viscosity at $\tilde{\sigma}_\beta$ and indicates the maximum flowable volume fraction at $\tilde{\sigma}_\beta$.

To estimate the shear-induced jamming point $\phi_{J,\beta}$, for suspensions of smooth and rough colloids, we invoke an argument that relates the divergence of η_r to $(\phi_J - \phi)$ at a given σ, where $\phi_J = \phi_J(\sigma)$. Specifically, the low-shear and high-shear viscosities are expected to diverge at ϕ_{max} and a σ-dependent ϕ_J, respectively, with an exponent of -2 [51]. By extension, this suggests that η_r at intermediate σ should also diverge to a corresponding stress-dependent quasi-jamming point, $\phi_{J,\beta} = \phi_{J,\beta}(\tilde{\sigma}_\beta)$ with the same exponent of -2. The inset in Fig. 4(b) shows the scaling of the

form $\eta_r \sim (\phi_{J,\beta} - \phi)^{-2}$, where $\phi_{J,\beta} = 0.61$ and 0.51 for smooth and rough colloids, respectively. The value of $z_{J,\beta}$ is then obtained by extrapolating $<z>_\beta$ at various ϕ to the respective quasi-jamming points $\phi_{J,\beta}$, where $z_{J,\beta}$ values are 4.95 ± 0.01 and 3.25 ± 0.01 for smooth and rough colloids. Figure 4(b) shows that the dynamic contact scaling takes the form $z^* \sim (\Delta\phi/\phi_{\max})^\alpha$ with $\alpha = 0.95 \pm 0.07$. A similar scaling ($\alpha = 1.08$) had been observed in 2D simulations of soft frictionless particles that are repulsive [52]. The observed power-law correlation in Fig. 4(b) is statistically significant with a normalized chi-squared parameter $\bar{\chi}^2 = 2.12$ and $P < 0.005$ [43,53].

In Fig. 1, following the vertical dashed lines corresponding to $\tilde{\sigma}_\beta$, an increase in ϕ is associated with an increase in β, and a decrease in both $\Delta\phi/\phi_{\max}$ and z^* is associated with the formation of more space-spanning contacts. For a given $\tilde{\sigma}_\beta$, for each particle system, there exists a $\phi_{J,\beta}$ and corresponding $z_{J,\beta}$ beyond which there is no steady state flow. In a constant volume rheological experiment restricted by the dimensions of experimental and simulation setup, the free volume available to rearrange under shear is greater for smooth colloids than that of the rough colloids, because smooth colloids can rotate freely with little hydrodynamic resistance [23,54]. The difference in spatial constraints imposed by the restricted rotational degree of freedom in rough colloids is captured by the deficiency of nearest neighbors to their respective $z_{J,\beta}$. The universality in Fig. 4(b) shows that this physical mechanism for shear thickening holds for all types of suspensions and thus the parameter z^*, which is a contact network parameter that captures the distance to $z_{J,\beta}$, can be used as a representation of the modes of particle motion under shear.

The dynamic contact scaling $z^* \sim \Delta\phi/\phi_{\max}$ [Fig. 4(b)] and the static packing correlation $\beta \sim \exp(-\Delta\phi/\phi_{\max})$ (Fig. 2) can be combined to relate the sheared contact microstructure and the shear thickening strength as $\beta \sim \exp(-z^*)$. The results suggest that at a given β, because $<z>$ is different for different suspension type, the force carried by each contact is different for particles of different morphologies. Earlier work on compressed hydrogel beads found that the macroscopic force, F, scales with dynamic contacts as $F \sim <z>$ [55]. To obtain the same change in suspension stress (or β), rough particles suspensions required, on average, fewer contacts compared to smooth particle suspensions. In other words, for the same F in our systems, $F/<z>$ for rough particle suspensions must be greater than that of the smooth counterpart. We indirectly capture the force per contact through the parameter z^*, which factors in the scaled contact deficit for various types of particle suspensions. Note that the contact networks found in this work would likely have different morphologies and properties from the force chains observed in previous studies [12]. The dynamic $<z>$ values in our studies act as scalar parameters that describe the collective particle rearrangement and their resultant microstructures under shear.

As a suspension shear thickens, clusters and percolated networks of particle contacts break and reform, but our study has shown that a mean-field description using dynamic $<z>$ can connect β and $\Delta\phi/\phi_{\max}$. The dynamic contact scaling may break down at ϕ values close to $\phi_{\max}$ ($\Delta\phi/\phi_{\max} \leq 10^{-2}$) due to pronounced flow instabilities [56–58] and the increase in uncertainty in z^* close to the jamming point could be due to these instabilities. Nonetheless, our study shows that the scaled jamming distance is a strong predictor for the shear thickening behavior of a broad class of colloidal suspensions.

Because force networks are likely coupled to the contact network and particle positions [59], future studies that analyze the transient network anisotropy could provide new insight as to how different types of particles carry load in flowing systems [60–62]. Athermal suspensions [63,64] and shape-anisotropic colloids [65] have not been tested in this study, and it would be interesting to see if the proposed scaling laws hold for these materials.

We thank John Brady, Ronald Larson, Jeffrey Morris, and Abhinendra Singh for discussions, and Rakshit Jain for VMD reconstructions. This work is supported in part by the National Science Foundation (CBET-1804462 and DMR-2104726), the American Chemical Society Petroleum Research Fund (ACS-PRF #59208-DNI9), and North Carolina State University start-up funds.

*Corresponding author.
lilian_hsiao@ncsu.edu

[1] E. Blanco, D. J. M. Hodgson, M. Hermes, R. Besseling, G. L. Hunter, P. M. Chaikin, M. E. Cates, I. Van Damme, and W. C. K. Poon, Proc. Natl. Acad. Sci. U.S.A. **116**, 10303 (2019).
[2] E. Brown, N. Rodenberg, J. Amend, A. Mozeika, E. Steltz, M. R. Zakin, H. Lipson, and H. M. Jaeger, Proc. Natl. Acad. Sci. U.S.A. **107**, 18809 (2010).
[3] Y. S. Lee, E. D. Wetzel, and N. J. Wagner, J. Mater. Sci. **38**, 2825 (2003).
[4] Y. Madraki, G. Ovarlez, and S. Hormozi, Phys. Rev. Lett. **121**, 108001 (2018).
[5] N. Y. C. Lin, C. Ness, M. E. Cates, J. Sun, and I. Cohen, Proc. Natl. Acad. Sci. U.S.A. **113**, 10774 (2016).
[6] C. S. O'Hern, L. E. Silbert, A. J. Liu, and S. R. Nagel, Phys. Rev. E **68**, 011306 (2003).
[7] I. R. Peters, S. Majumdar, and H. M. Jaeger, Nature (London) **532**, 214 (2016).
[8] J. F. Brady and G. Bossis, Annu. Rev. Fluid Mech. **20**, 111 (1988).
[9] J. Bender and N. J. Wagner, J. Rheol. **40**, 899 (1996).
[38] L. C. Hsiao, S. Jamali, E. Glynos, P. F. Green, R. G. Larson, and M. J. Solomon, Phys. Rev. Lett. **119**, 158001 (2017).
[10] J. F. Morris, Phys. Rev. Fluids **3**, 110508 (2018).
[11] S. Jamali and J. F. Brady, Phys. Rev. Lett. **123**, 138002 (2019).

[12] J. E. Thomas, K. Ramola, A. Singh, R. Mari, J. F. Morris, and B. Chakraborty, Phys. Rev. Lett. **121**, 128002 (2018).
[13] E. Brown and H. M. Jaeger, Rep. Prog. Phys. **77**, 046602 (2014).
[14] M. Wang, S. Jamali, and J. F. Brady, J. Rheol. **64**, 379 (2020).
[15] R. J. E. Andrade, A. R. Jacob, F. J. Galindo-Rosales, L. Campo-Deaño, Q. Huang, O. Hassager, and G. Petekidis, J. Rheol. **64**, 1179 (2020).
[16] A. K. Gurnon and N. J. Wagner, J. Fluid Mech. **769**, 242 (2015).
[17] E. Somfai, M. van Hecke, W. G. Ellenbroek, K. Shundyak, and W. van Saarloos, Phys. Rev. E **75**, 020301(R) (2007).
[18] L. E. Silbert, Soft Matter **6**, 2918 (2010).
[19] A. Singh, C. Ness, R. Seto, J. J. de Pablo, and H. M. Jaeger, Phys. Rev. Lett. **124**, 248005 (2020).
[20] M. Wyart and M. E. Cates, Phys. Rev. Lett. **112**, 098302 (2014).
[21] R. Seto, R. Mari, J. F. Morris, and M. M. Denn, Phys. Rev. Lett. **111**, 218301 (2013).
[22] A. Singh, R. Mari, M. M. Denn, and J. F. Morris, J. Rheol. **62**, 457 (2018).
[23] L. C. Hsiao, I. Saha-Dalal, R. G. Larson, and M. J. Solomon, Soft Matter **13**, 9229 (2017).
[24] S. Jiang, J. Yan, J. K. Whitmer, S. M. Anthony, E. Luijten, and S. Granick, Phys. Rev. Lett. **112**, 218301 (2014).
[25] K. V. Edmond, M. T. Elsesser, G. L. Hunter, D. J. Pine, and E. R. Weeks, Proc. Natl. Acad. Sci. U.S.A. **109**, 17891 (2012).
[26] L. C. Hsiao and S. Pradeep, Curr. Opin. Colloid Interface Sci. **43**, 94 (2019).
[27] Y. Peng, C. M. Serfass, C. N. Hill, and L. C. Hsiao, Exp. Mech. **61**, 969 (2021).
[28] Y. Peng, C. M. Serfass, A. Kawazoe, Y. Shao, K. Gutierrez, C. N. Hill, V. J. Santos, Y. Visell, and L. C. Hsiao, Nat. Mater. (2021), https://doi.org/10.1038/s41563-021-00990-9.
[29] S. Pradeep and L. C. Hsiao, Soft Matter **16**, 4980 (2020).
[30] M. T. Elsesser and A. D. Hollingsworth, Langmuir **26**, 17989 (2010).
[31] J. C. Crocker and D. G. Grier, J. Colloid Interface Sci. **179**, 298 (1996).
[32] D. A. Fedosov, W. Pan, B. Caswell, G. Gompper, and G. E. Karniadakis, Proc. Natl. Acad. Sci. U.S.A. **108**, 11772 (2011).
[33] R. Mari, R. Seto, J. F. Morris, and M. M. Denn, Proc. Natl. Acad. Sci. U.S.A. **112**, 15326 (2015).
[34] B. M. Guy, M. Hermes, and W. C. K. Poon, Phys. Rev. Lett. **115**, 088304 (2015).
[35] B. M. Guy, C. Ness, M. Hermes, L. J. Sawiak, J. Sun, and W. C. K. Poon, Soft Matter **16**, 229 (2020).
[36] C. D. Cwalina and N. J. Wagner, J. Rheol. **58**, 949 (2014).
[37] O. Sedes, A. Singh, and J. F. Morris, J. Rheol. **64**, 309 (2020).
[39] C. P. Hsu, S. N. Ramakrishna, M. Zanini, N. D. Spencer, and L. Isa, Proc. Natl. Acad. Sci. U.S.A. **115**, 5117 (2018).
[40] D. Lootens, H. van Damme, Y. Hémar, and P. Hébraud, Phys. Rev. Lett. **95**, 268302 (2005).
[41] J. R. Royer, D. L. Blair, and S. D. Hudson, Phys. Rev. Lett. **116**, 188301 (2016).
[42] S. K. Dutta, A. Mbi, R. C. Arevalo, and D. L. Blair, Rev. Sci. Instrum. **84**, 063702 (2013).
[43] See Supplemental Material at http://link.aps.org/supplemental/10.1103/PhysRevLett.127.158002 for details regarding microstructure photoarresting protocol, DPD simulations, contact criterion model, and statistical analysis.
[44] R. Kubo, Rep. Prog. Phys. **29**, 255 (1966).
[45] A. Boromand, S. Jamali, B. Grove, and J. M. Maia, J. Rheol. **62**, 905 (2018).
[46] S. Jamali, A. Boromand, N. Wagner, and J. Maia, J. Rheol. **59**, 1377 (2015).
[47] A. Boromand, S. Jamali, and J. M. Maia, Comput. Phys. Commun. **196**, 149 (2015).
[48] J. R. Melrose and R. C. Ball, Europhys. Lett. **32**, 535 (1995).
[49] Yu-FanLee, YiminLuo, TianyiBai, C. Velez, S. C. Brown, and N. J. Wagner, Phys. Fluids **33**, 033316 (2021).
[50] V. Kobelev and K. S. Schweizer, Phys. Rev. E **71**, 021401 (2005).
[51] M. Wang and J. F. Brady, Phys. Rev. Lett. **115**, 158301 (2015).
[52] M. Maiti, H. A. Vinutha, S. Sastry, and C. Heussinger, J. Chem. Phys. **143**, 144502 (2015).
[53] J. R. Taylor, *An Introduction to Error Analysis: The Study of Uncertainities in Physical Measurements*, 2nd ed. (University Science Books, Sausalito, CA, 1997).
[54] A. Singh, G. L. Jackson, M. van der Naald, J. J. de Pablo, and H. M. Jaeger, arXiv:2108.09860.
[55] N. Brodu, J. A. Dijksman, and R. P. Behringer, Nat. Commun. **6**, 6361 (2015).
[56] G. Ovarlez, A. Vu Nguyen Le, W. J. Smit, A. Fall, R. Mari, G. Chatté, and A. Colin, Sci. Adv. **6**, eaay5589 (2020).
[57] S. Saw, M. Grob, A. Zippelius, and C. Heussinger, Phys. Rev. E **101**, 012602 (2020).
[58] V. Rathee, D. L. Blair, and J. S. Urbach, Proc. Natl. Acad. Sci. U.S.A. **114**, 8740 (2017).
[59] R. P. Behringer and B. Chakraborty, Rep. Prog. Phys. **82**, 012601 (2019).
[60] M. Gameiro, A. Singh, L. Kondic, K. Mischaikow, and J. F. Morris, Phys. Rev. Fluids **5**, 034307 (2020).
[61] L. E. Edens, E. G. Alvarado, A. Singh, J. F. Morris, G. K. Schenter, J. Chun, and A. E. Clark, Soft Matter **17**, 7476 (2021).
[62] O. Sedes, B. Chakraborty, H. A. Makse, and J. F. Morris, arXiv:2108.07261.
[63] A. Fall, N. Huang, F. Bertrand, G. Ovarlez, and D. Bonn, Phys. Rev. Lett. **100**, 018301 (2008).
[64] F. Picano, W.-P. Breugem, D. Mitra, and L. Brandt, Phys. Rev. Lett. **111**, 098302 (2013).
[65] L. Palangetic, K. Feldman, R. Schaller, R. Kalt, W. R. Caseri, and J. Vermant, Faraday Discuss. **191**, 325 (2016).